



Published in final edited form as:

J Mol Biol. 2011 October 14; 413(1): 17–23. doi:10.1016/j.jmb.2011.08.036.

Characterization of a Myosin VII MyTH/FERM domain

Rebecca J. Moen¹, Daniel O. Johnsrud², David D. Thomas¹, and Margaret A. Titus^{2,*}

¹Department of Biochemistry, Molecular Biology and Biophysics, University of Minnesota, Minneapolis, MN 55455

²Department of Genetics, Cell Biology and Development, University of Minnesota, Minneapolis, MN 55455

Abstract

A group of closely related myosins are characterized by the presence of at least one MyTH/FERM (myosin talin homology 4; band 4.1, ezrin, radixin, moesin) domain in their C-terminal tails. This domain interacts with a variety of binding partners, and mutations in either the MyTH4 or FERM domains of myosin VII and XV result in deafness, highlighting the functional importance of each domain. The N-terminal MyTH/FERM region of *Dictyostelium* myosin VII (M7) has been isolated as a first step toward gaining insight into the function of this domain and its interaction with binding partners. The M7 MyTH4/FERM domain (MF1) binds to both actin and microtubules in vitro, with dissociation constants of 13.7 and 1.7 μM , respectively. Gel filtration and UV spectroscopy reveal that MF1 exists as a monomer in solution and forms a well-folded, compact conformation with a high degree of secondary structure. These results indicate that MF1 forms an integrated structural domain that serves to couple actin filaments and microtubules in specific regions of the cytoskeleton.

Keywords

MyTH4; FERM; myosin 7; microtubules; actin

Unconventional myosins have diverse cellular roles that are dictated, in large part, by class-specific tail domains that target each motor to specific cargo or subcellular locations. A subgroup of these motors, myosin VII (M7), myosin X (M10) and myosin XV (M15), is referred to as MyTH/FERM myosins because of the presence of one or two MyTH/FERM domains (myosin talin homology 4; band 4.1, ezrin, radixin, moesin) in their C-termini. The MyTH/FERM myosins are closely related both phylogenetically and functionally - for example, all MyTH/FERM myosins are localized to the tips of actin-rich projections such as filopodia or stereocilia and play a role in the extension of these structures^{1; 2; 3; 4}. MyTH/FERM domains are also found in other motors and proteins with roles in cytoskeletal function, including a plant kinesin and MAX-1^{5; 6}. While solo FERM domains are found in a large number of proteins, including talin and focal adhesion kinase, MyTH4 domains are frequently N-terminal to a FERM domain, suggesting a functional integration of the two. The importance of the myosin MyTH/FERM domain is highlighted by the finding that

© 2011 Elsevier Ltd. All rights reserved.

Address correspondence to: Margaret A. Titus, Department of Genetics, Cell Biology and Development, 6-160 Jackson Hall, 321 Church St. SE, University of Minnesota, Minneapolis, MN 55455. T: (612) 625-8498, F: (612) 625-4648, titus004@umn.edu.

Publisher's Disclaimer: This is a PDF file of an unedited manuscript that has been accepted for publication. As a service to our customers we are providing this early version of the manuscript. The manuscript will undergo copyediting, typesetting, and review of the resulting proof before it is published in its final citable form. Please note that during the production process errors may be discovered which could affect the content, and all legal disclaimers that apply to the journal pertain.

mutations in either the MyTH4 or FERM domains of M7a and M15a result in deafness in human patients ^{7; 8; 9; 10}.

The MyTH/FERM domains of M7, M10 and M15 interact with a variety of proteins, including both microtubules and actin. A plant kinesin MyTH4 domain cosediments with microtubules ⁶, and the combined MyTH/FERM domains of human and *Xenopus* M10 interact with microtubules ^{11; 12}. M10 colocalizes with microtubules in the meiotic spindle of *Xenopus* oocytes, is found at mitotic spindle poles in embryos ^{11; 13} and is required for correct mitotic spindle orientation ^{13; 14}. The isolated C-terminal FERM domain of *Drosophila* M7a binds actin with moderate affinity ($\sim 30 \mu\text{M}$) ¹⁵ and the FERM domain of a *Tetrahymena* MyTH/FERM myosin is found in actin immunoprecipitates ¹⁶. The tails of these myosins can thus bind to either actin or microtubules, enabling them to slide actin against either microtubules or another actin filament or even tether actin or microtubules to actin.

Detailed characterization of the biophysical and structural properties of the MyTH/FERM domain, along with the ability to determine the nature of its interaction with partner proteins that serve to anchor or regulate myosin activity, is necessary to fully understand MyTH/FERM myosin function, as well as the role of other proteins that have this domain. The social amoeba *Dictyostelium* expresses a class 7 myosin (DdM7) that contains two MyTH/FERM domains separated by an SH3 domain ¹⁷. This myosin is required for filopod extension and cell-substrate adhesion, roles quite similar to those described for M10 ^{1; 2; 17; 18}. The tail domain of DdM7 interacts specifically with another FERM domain protein required for adhesion, talinA, ¹⁹ which modulates the dynamic membrane association of DdM7 ²⁰. The contribution of the MyTH/FERM domains to DdM7 function is not yet known. In the present study, the ability to readily express protein domains fused to the motor domain of myosin II ²¹ was exploited to purify and characterize the N-terminal MyTH/FERM domain of DdM7 as a first step toward a more detailed understanding of this combined domain and its interaction with both actin and microtubules.

Isolation of the DdM7 N-terminal MyTH4/FERM domain

The N-terminal MyTH4/FERM domain of DdM7 (MF1 - residues 1085–1620) (Fig. 1A) was fused to the C-terminal end of the myosin II motor domain (S1) ²¹ and after lysis under rigor conditions, the fusion was highly enriched in the cytoskeleton fraction (Fig. 1B). Following release from the cytoskeleton with MgATP, cleavage from S1 with TEV and metal affinity chromatography, purified MF1 was obtained (Fig. 1B) and its identity confirmed by mass spectrometry (Fig. 1C).

MF1 binding to F-actin

FERM domains are considered to interact primarily with the cytoplasmic tails of membrane receptors. It has only recently been appreciated that they can also bind directly to F-actin ^{15; 22}. The talin FERM domain interacts directly with actin and while the affinity is not known, it has been suggested that it is sufficient to account for the interaction of talin to actin ²². The affinity of MF1 for actin was measured by cosedimentation ²³ and the binding curve reveals a single K_d of $13.7 \pm 2.6 \mu\text{M}$ (Fig. 2). The finding that MF1 has a nearly 2-fold greater K_d for actin binding, in comparison to the fly M7a C-terminal FERM domain ($\sim 30 \mu\text{M}$) ¹⁵, suggests that the MyTH4 domain could increase the binding affinity, possibly by causing the actin-binding sequence to be more exposed and accessible. These results indicate that the FERM-actin interaction is conserved but generally of low affinity. However, the existence of two domains within the M7 molecule that interact weakly with F-actin would result in stronger overall actin binding.

MF1 binding to Microtubules

The interaction of myosin MyTH4 domains with microtubules is known, but the binding strength has not been measured. The interaction of MF1 with microtubules was assayed by cosedimentation²⁴ and the resulting binding curve yields a single K_d of $1.7 \pm 0.5 \mu\text{M}$ (Fig. 3), indicating a stronger affinity for microtubules than for actin. The curve unexpectedly showed saturation at 0.25 fraction bound, initially suggesting that a significant portion of the MF1 preparation was unable to interact with microtubules. A similar low binding saturation was observed for the actoMF1 interaction (Fig. 2). The supernatant from the highest tubulin concentration ($10 \mu\text{M}$) was recovered, additional microtubules added ($10 \mu\text{M}$ tubulin, final concentration) and the sample re-centrifuged (Fig. 3). Approximately 25% of MF1 from the supernatant cosedimented with the microtubules, as observed in the initial binding assay (Fig. 3B), indicating that the low overall saturation binding was not due to a large fraction of the preparation being denatured. These results show clearly that the isolated MF1 domain is in equilibrium between two conformational states, one of which does not bind to microtubules or actin and one that does.

Overall MF1 Structure and Stability

The crystal structures of two myosin MyTH/FERM domains in association with known binding partner peptides have recently been solved^{12; 25; 26}. The MyTH4 domain is a bundle of helices, 6 of which are highly conserved. The FERM domain, consistent with previously published x-ray and NMR studies of FERM domains from talin, radixin, moesin, merlin, and protein 4.1R^{27; 28; 29}, adopts the canonical three-lobe cloverleaf structure, with the three subdomains denoted F1, F2, and F3. In both the M7a and M10 MyTH/FERM structures, the MyTH4 and FERM domains interact with one another, forming a functional and structural supramodule. Consistent with these findings, gel filtration analysis of the purified MF1 reveals that it is a tightly folded monomer with a calculated Stokes radius of $2.74 \pm 0.34 \text{ nm}$ (Fig. 4A). The far-UV circular dichroism (CD) spectrum of MF1 also confirms that it is a highly helical protein with intense CD bands at both 208 nm and 222 nm (Fig. 4B). Analysis of the CD spectrum, using CDPPro Analysis³⁰, yielded an estimated secondary structure of $55\% \pm 3\%$ α -helix and $21\% \pm 4\%$ β -sheet. The thermal unfolding of MF1 secondary structure occurred in one transition, with an onset of unfolding at $\sim 35^\circ\text{C}$ and a transition midpoint (T_m) at 42°C (Fig. 4C). The sharp transition indicates highly cooperative unfolding of MF1.

The secondary structure of the mammalian M7a and M10 MyTH/FERM domains are 46% α -helix/15% β -sheet and 49% α -helix/14% β -sheet, respectively (determined using STRIDE³¹ and Protein Data Bank files 3PVL and 3PZD). The α -helix and β -sheet content of DdM7 MF1 are predicted to be slightly higher than calculated for mammalian M7a and M10, with $55\% \pm 3\%$ α -helix and $21\% \pm 4\%$ β -sheet based on fitting of the far-UV CD spectrum (Fig. 4B). The differences in secondary structure may be attributed to the sequence divergence between amoeba and vertebrate MyTH/FERM domains and/or that MF1 exists in the apo state.

The amoeba *Dictyostelium discoideum* is evolutionary quite distant from vertebrates³². A comparison of the MyTH-FERM domain sequences from mouse M7a (residues 993–1567, GenBank AAB40708.1) and human M10 (residues 1503–2047, GenBank AAF68025.2) to DdM7 MF1 reveals a low sequence identity of 20% for both and sequence homology of 36% and 39%, respectively. Sequence alignment reveals the DdM7 N-terminal MyTH4 sequence is substantially shorter than both the M7a and M10 MyTH4 sequences. The missing sequence of DdM7 encompasses helices 3 and 4 of the mammalian M7a MyTH

domain, suggesting that the DdM7 MF1 MyTH4 structure differs slightly from that of M7a, although the 6-helix core is predicted to remain intact²⁵.

A positively charged patch on the MyTH4 domain of human M10 consisting of eight positively charged residues has been implicated in MT binding²⁶. Consistent with this possibility, mutation of two of these (K1647 and K1650) is sufficient to abolish all binding to tubulin acidic tails¹². Three of these eight positively charged residues are conserved between the human M10 and DdM7 MF1 MyTH4 domains (R1643, K1647, K1654 in M10; R1257, K1261, and K1268 in DdM7), suggesting that MF1 may also bind to MTs by a similar electrostatic interaction.

Conclusion

MyTH/FERM domains are present in numerous cytoskeletal signaling and motor proteins and much remains to be learned about their combined structure and function. The structure of MyTH/FERM domains is predicted to be conserved throughout evolution despite a high degree of sequence divergence of these domains. The ability of MF1 to bind both actin and microtubules suggests an important role for this domain in linking cytoskeletal elements. M7 and M10 are localized to regions of the cell where actin and microtubules are both present^{11; 33}. M10 and M15 can link microtubule-based structures to actin,^{11; 13; 14; 34} but the contribution of microtubule binding to M7 activity is not yet clear. Fly M7a is monomeric in vitro and most likely exists in a folded conformation, with the FERM domain interacting with and inhibiting the motor domain¹⁵. The MyTH/FERM regions might be partially or fully blocked from binding to microtubules or actin in this configuration. Consistent with this possibility is the observation that DdM7 is largely cytosolic^{1; 19}. Activation of the folded myosin, either by as yet unknown regulatory factors that dimerize M7³⁵ or the presence of high local concentrations of either actin or microtubules, might expose these sites. Our data also suggest an alternative mechanism, in which there exist two conformations of the MyTH/FERM domain itself, only one of which is available for actin or microtubule binding. This poised equilibrium is an obvious target for regulatory control, as shown recently for the myosin regulatory light chain³⁶. Once the binding sites are available, the tail could interact with both actin and microtubules, enabling cortical DdM7 to actively stabilize the leading edge of the cells by strengthening cell-substrate adhesions.

Supplementary Material

Refer to Web version on PubMed Central for supplementary material.

Acknowledgments

We thank Dr. Ewa Prochniewicz for expert advice on actin binding measurements, Drs. Holly Goodson (Notre Dame) and Susan Gilbert (RPI) for help with microtubule binding experiments, Dr. Martin Kollmar (Max Planck Institute) for the pDXA-mako 4b expression plasmid, Eunice Song for technical assistance, and Drs. Anne Houdusse (Institute Curie) and Gaku Ashiba for many helpful discussions. CD spectroscopy was performed at the Biophysical Spectroscopy Facility, University of Minnesota. We appreciate the excellent assistance with manuscript preparation from Octavian Cornea. This work was supported by NIH grants GM046486 (ARRA award) to MAT, AR032961 to DDT and F31AG037303 to RJM.

ABBREVIATIONS

MyTH4	myosin tail homology 4
FERM	band 4.1, ezrin, radixin, moesin
DdM7	<i>Dictyostelium discoideum</i> myosin 7

MF1 *Dictyostelium* myosin 7 N-terminal MyTH4/FERM domain

LITERATURE CITED

1. Tuxworth RI, Weber I, Wessels D, Addicks GC, Soll DR, Gerisch G, Titus MA. A role for myosin VII in dynamic cell adhesion. *Curr Biol.* 2001; 11:318–29. [PubMed: 11267868]
2. Bohil AB, Robertson BW, Cheney RE. Myosin-X is a molecular motor that functions in filopodia formation. *Proc Natl Acad Sci U S A.* 2006; 103:12411–6. [PubMed: 16894163]
3. Belyantseva IA, Boger ET, Naz S, Frolenkov GI, Sellers JR, Ahmed ZM, Griffith AJ, Friedman TB. Myosin-XVa is required for tip localization of whirlin and differential elongation of hair-cell stereocilia. *Nat Cell Biol.* 2005; 7:148–56. [PubMed: 15654330]
4. Prosser HM, Rzadzinska AK, Steel KP, Bradley A. Mosaic complementation demonstrates a regulatory role for myosin VIIa in actin dynamics of stereocilia. *Mol Cell Biol.* 2008; 28:1702–12. [PubMed: 18160714]
5. Huang X, Cheng HJ, Tessier-Lavigne M, Jin Y. MAX-1, a novel PH/MyTH4/FERM domain cytoplasmic protein implicated in netrin-mediated axon repulsion. *Neuron.* 2002; 34:563–76. [PubMed: 12062040]
6. Narasimhulu SB, Reddy AS. Characterization of microtubule binding domains in the *Arabidopsis* kinesin-like calmodulin binding protein. *Plant Cell.* 1998; 10:957–65. [PubMed: 9634584]
7. Jaijo T, Aller E, Beneyto M, Najera C, Graziano C, Turchetti D, Seri M, Ayuso C, Baiget M, Moreno F, Morera C, Perez-Garrigues H, Millan JM. MYO7A mutation screening in Usher syndrome type I patients from diverse origins. *J Med Genet.* 2007; 44:e71. [PubMed: 17361009]
8. Liburd N, Ghosh M, Riazuddin S, Naz S, Khan S, Ahmed Z, Liang Y, Menon PS, Smith T, Smith AC, Chen KS, Lupski JR, Wilcox ER, Potocki L, Friedman TB. Novel mutations of MYO15A associated with profound deafness in consanguineous families and moderately severe hearing loss in a patient with Smith-Magenis syndrome. *Hum Genet.* 2001; 109:535–41. [PubMed: 11735029]
9. Riazuddin S, Nazli S, Ahmed ZM, Yang Y, Zulfiqar F, Shaikh RS, Zafar AU, Khan SN, Sabar F, Javid FT, Wilcox ER, Tsilou E, Boger ET, Sellers JR, Belyantseva IA, Friedman TB. Mutation spectrum of MYO7A and evaluation of a novel nonsyndromic deafness DFNB2 allele with residual function. *Hum Mutat.* 2008; 29:502–11. [PubMed: 18181211]
10. Wang A, Liang Y, Fridell RA, Probst FJ, Wilcox ER, Touchman JW, Morton CC, Morell RJ, Noben-Trauth K, Camper SA, Friedman TB. Association of unconventional myosin MYO15 mutations with human nonsyndromic deafness DFNB3. *Science.* 1998; 280:1447–51. [PubMed: 9603736]
11. Weber KL, Sokac AM, Berg JS, Cheney RE, Bement WM. A microtubule-binding myosin required for nuclear anchoring and spindle assembly. *Nature.* 2004; 431:325–9. [PubMed: 15372037]
12. Hirano Y, Hatano T, Takahashi A, Toriyama M, Inagaki N, Hakoshima T. Structural basis of cargo recognition by the myosin-X MyTH4-FERM domain. *Embo J.* 2011
13. Woolner S, O'Brien LL, Wiese C, Bement WM. Myosin-10 and actin filaments are essential for mitotic spindle function. *J Cell Biol.* 2008; 182:77–88. [PubMed: 18606852]
14. Toyoshima F, Nishida E. Integrin-mediated adhesion orients the spindle parallel to the substratum in an EB1- and myosin X-dependent manner. *EMBO J.* 2007; 26:1487–98. [PubMed: 17318179]
15. Yang Y, Baboolal TG, Siththanandan V, Chen M, Walker ML, Knight PJ, Peckham M, Sellers JR. A FERM domain autoregulates *Drosophila* myosin 7a activity. *Proc Natl Acad Sci U S A.* 2009; 106:4189–94. [PubMed: 19255446]
16. Gotesman M, Hosein RE, Gavin RH. A FERM domain in a class XIV myosin interacts with actin and tubulin and localizes to the cytoskeleton, phagosomes, and nucleus in *Tetrahymena thermophila*. *Cytoskeleton (Hoboken).* 67:90–101. [PubMed: 20169533]
17. Titus MA. A class VII unconventional myosin is required for phagocytosis. *Curr Biol.* 1999; 9:1297–303. [PubMed: 10574761]

18. Zhang H, Berg JS, Li Z, Wang Y, Lang P, Sousa AD, Bhaskar A, Cheney RE, Stromblad S. Myosin-X provides a motor-based link between integrins and the cytoskeleton. *Nat Cell Biol.* 2004; 6:523–31. [PubMed: 15156152]
19. Tuxworth RI, Stephens S, Ryan ZC, Titus MA. Identification of a myosin VII-talin complex. *J Biol Chem.* 2005; 280:26557–64. [PubMed: 15826949]
20. Galdeen SA, Stephens S, Thomas DD, Titus MA. Talin influences the dynamics of the myosin VII-membrane interaction. *Mol Biol Cell.* 2007; 18:4074–84. [PubMed: 17671169]
21. Kollmar M. Use of the myosin motor domain as large-affinity tag for the expression and purification of proteins in *Dictyostelium discoideum*. *Int J Biol Macromol.* 2006; 39:37–44. [PubMed: 16516959]
22. Lee HS, Bellin RM, Walker DL, Patel B, Powers P, Liu H, Garcia-Alvarez B, de Pereda JM, Liddington RC, Volkmann N, Hanein D, Critchley DR, Robson RM. Characterization of an actin-binding site within the talin FERM domain. *J Mol Biol.* 2004; 343:771–84. [PubMed: 15465061]
23. Prochniewicz E, Thomas DD. Site-specific mutations in the myosin binding sites of actin affect structural transitions that control myosin binding. *Biochemistry.* 2001; 40:13933–40. [PubMed: 11705383]
24. Allingham JS, Sproul LR, Rayment I, Gilbert SP. Vik1 modulates microtubule-Kar3 interactions through a motor domain that lacks an active site. *Cell.* 2007; 128:1161–72. [PubMed: 17382884]
25. Wu L, Pan L, Wei Z, Zhang M. Structure of MyTH4-FERM domains in myosin VIIa tail bound to cargo. *Science.* 2011; 331:757–60. [PubMed: 21311020]
26. Wei Z, Yan J, Lu Q, Pan L, Zhang M. Cargo recognition mechanism of myosin X revealed by the structure of its tail MyTH4-FERM tandem in complex with the DCC P3 domain. *Proc Natl Acad Sci U S A.* 2011; 108:3572–7. [PubMed: 21321230]
27. Han BG, Nunomura W, Takakuwa Y, Mohandas N, Jap BK. Protein 4.1R core domain structure and insights into regulation of cytoskeletal organization. *Nat Struct Biol.* 2000; 7:871–5. [PubMed: 11017195]
28. Hamada K, Shimizu T, Matsui T, Tsukita S, Hakoshima T. Structural basis of the membrane-targeting and unmasking mechanisms of the radixin FERM domain. *Embo J.* 2000; 19:4449–62. [PubMed: 10970839]
29. Pearson MA, Reczek D, Bretscher A, Karplus PA. Structure of the ERM protein moesin reveals the FERM domain fold masked by an extended actin binding tail domain. *Cell.* 2000; 101:259–70. [PubMed: 10847681]
30. Sreerama N, Woody RW. Estimation of protein secondary structure from circular dichroism spectra: comparison of CONTIN, SELCON, and CDSSTR methods with an expanded reference set. *Anal Biochem.* 2000; 287:252–60. [PubMed: 11112271]
31. Heinig M, Frishman D. STRIDE: a web server for secondary structure assignment from known atomic coordinates of proteins. *Nucleic Acids Res.* 2004; 32:W500–2. [PubMed: 15215436]
32. Schaap P, Winckler T, Nelson M, Alvarez-Curto E, Elgie B, Hagiwara H, Cavender J, Milano-Curto A, Rozen DE, Dingermann T, Mutzel R, Baldauf SL. Molecular phylogeny and evolution of morphology in the social amoebas. *Science.* 2006; 314:661–3. [PubMed: 17068267]
33. Wolfrum U, Liu X, Schmitt A, Udovichenko IP, Williams DS. Myosin VIIa as a common component of cilia and microvilli. *Cell Motil Cytoskeleton.* 1998; 40:261–71. [PubMed: 9678669]
34. Kwon M, Godinho SA, Chandhok NS, Ganem NJ, Azioune A, They M, Pellman D. Mechanisms to suppress multipolar divisions in cancer cells with extra centrosomes. *Genes Dev.* 2008; 22:2189–203. [PubMed: 18662975]
35. Sakai T, Umeki N, Ikebe R, Ikebe M. Cargo binding activates myosin VIIA motor function in cells. *Proc Natl Acad Sci U S A.* 2011; 108:7028–33. [PubMed: 21482763]
36. Kast D, Espinoza-Fonseca LM, Yi C, Thomas DD. Phosphorylation-induced structural changes in smooth muscle myosin regulatory light chain. *Proc Natl Acad Sci U S A.* 2010; 107:8207–12. [PubMed: 20404208]

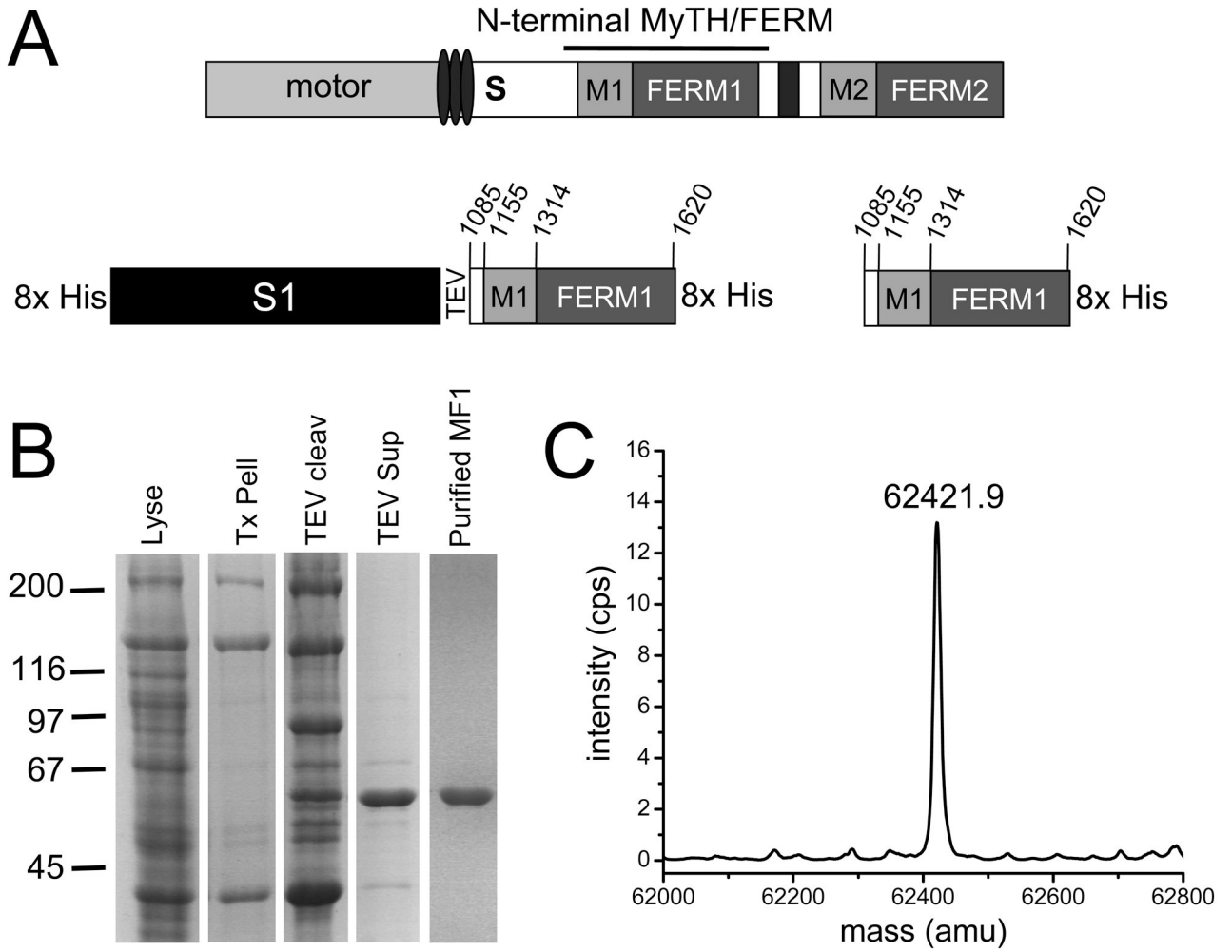


FIGURE 1. Isolation of the N-terminal MyTH/FERM domain of DdM7
 (A) Schematic illustration of DdM7 highlighting the major domains, including the IQ motifs (ovals), single alpha-helix (S), N-terminal MyTH/FERM domain (M1, FERM1), SH3 domain (black rectangle) and C-terminal MyTH/FERM domain (M2, FERM2). The S1-MF1 fusion is also shown, with the myosin II motor domain (S1) and the locations of the TEV cleavage site and His tags indicated. The S1-MF1 fusion was generated using a modified pDXA-mako 4b expression plasmid²¹. (B) Purification of MF1 as monitored by SDS-PAGE. Coomassie stained gel showing the total cell lysate (Lyse), rigor cytoskeleton (Tx Pell), cytoskeleton following TEV cleavage (TEV cleav), soluble fraction following centrifugation of the cleaved cytoskeleton pellet (TEV sup) and purified MF1. Details of MF1 purification are provided in Supplementary Information. (C) Determination of the molecular mass of MF1 by ESI MS.

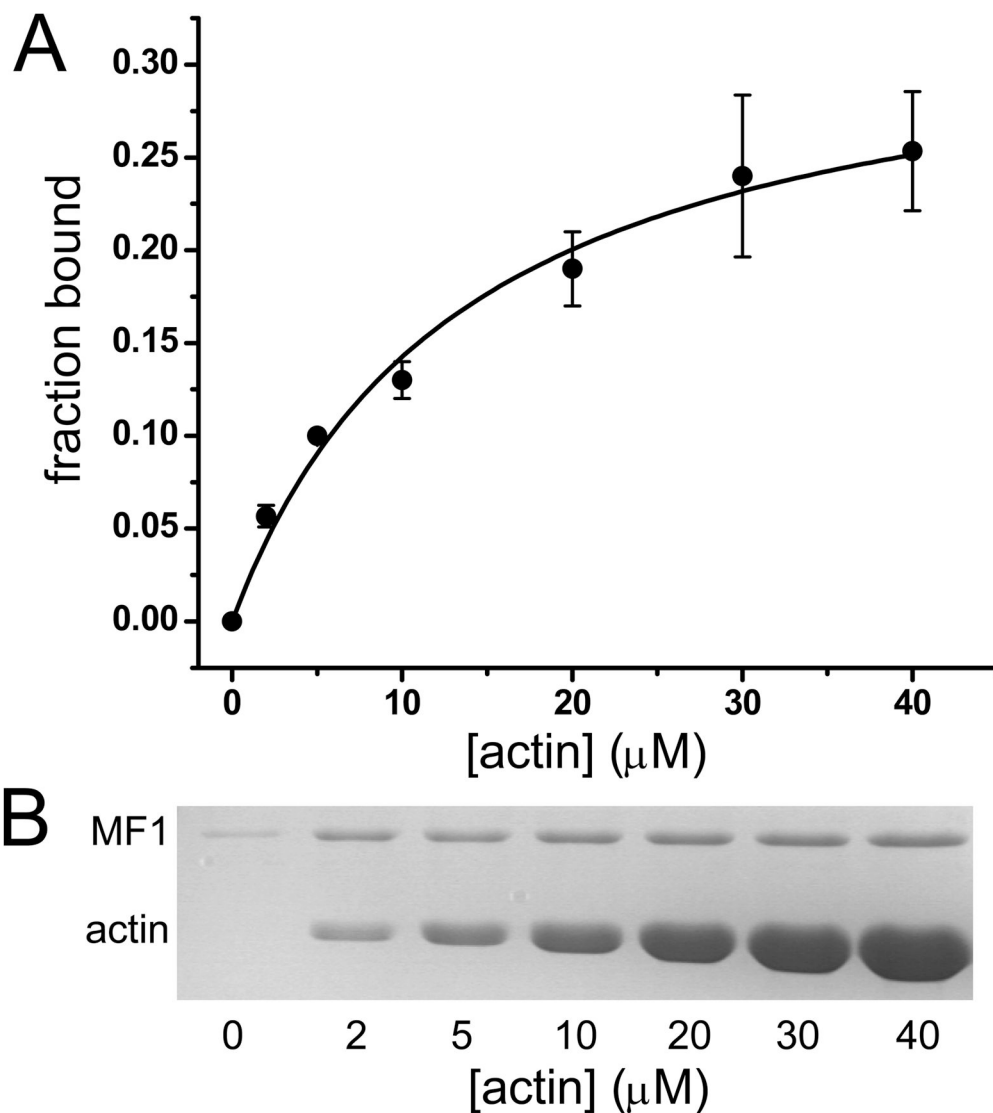


FIGURE 2. Binding of MF1 to actin

(A) Fraction bound MF1 with increasing actin concentration. Data was fit to a hyperbola yielding $K_d = 13.7 \pm 2.6 \mu\text{M}$. Data shown represent three independent experiments. (B) Data in A were obtained from SDS-PAGE of pellets from cosedimentation of MF1 with actin. Binding assays were performed by mixing increasing concentrations of actin with $2.5 \mu\text{M}$ MF1 in 10 mM imidazole, 2 mM MgCl_2 , 1 mM ATP, 0.1 mM DTT pH 7.5 buffer followed by centrifugation at $340,000 \times g$ using a TLA100.3 rotor (Beckman Coulter) to pellet the actoMF1 complex. Supernatant and pellet samples were run on 10% SDS-PAGE gels that were stained with Coomassie G and band intensity analyzed by densitometry using Image J.

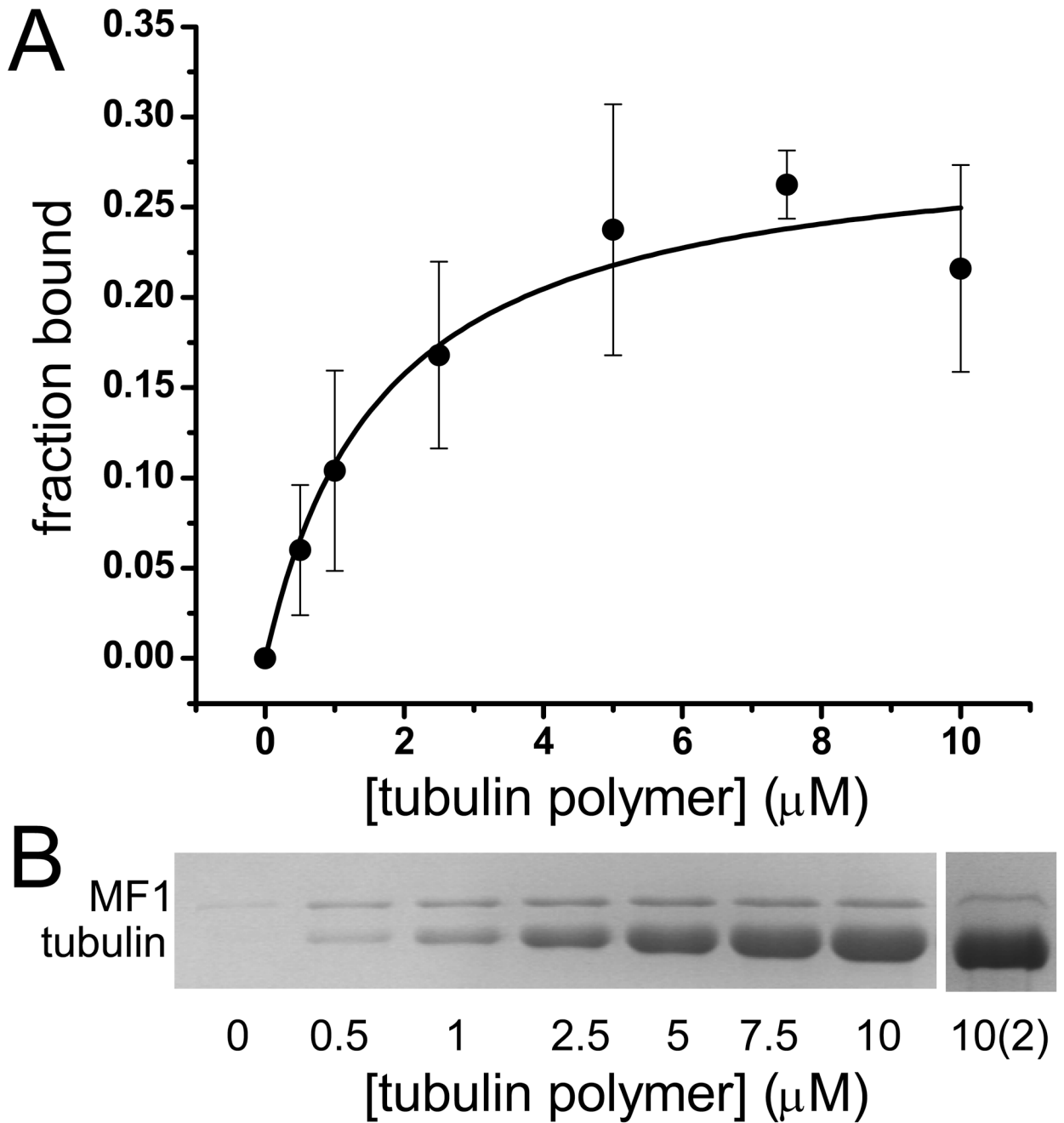


FIGURE 3. Binding of MF1 to tubulin

(A) Fraction bound MF1 with increasing tubulin heterodimer concentrations. Data was fit to a hyperbola, yielding $K_d = 1.7 \pm 0.5 \mu\text{M}$. Data represent five independent experiments. (B) Data in A were obtained from SDS-PAGE of pellets from a representative cosedimentation experiment. Sample 10(2) shows the cosedimentation of unbound MF1 to microtubules after initial binding assay. Microtubule binding assays were performed by mixing increasing μM concentrations of tubulin (Cytoskeleton (Denver, CO) or gift from Dr. Holly Davidson, Notre Dame) with $2.5 \mu\text{M}$ MF1 in 10 mM PIPES, 5 mM MgCl_2 , 1 mM EGTA, pH 7.0 buffer, incubated for 30 min at room temperature, followed by centrifugation at $90,000 \times g$ for 10 min at 25°C to pellet the tubulin-MF1 complex. The pellet was resuspended in 10

mM PIPES, 5 mM MgCl₂, 1 mM EGTA, 5 mM CaCl₂ pH 7.0 at 4°C, allowing MTs to depolymerize. Supernatant and pellet samples were run on 10% SDS-PAGE gels that were stained with Coomassie G. Band intensities were analyzed by densitometry using Image J.

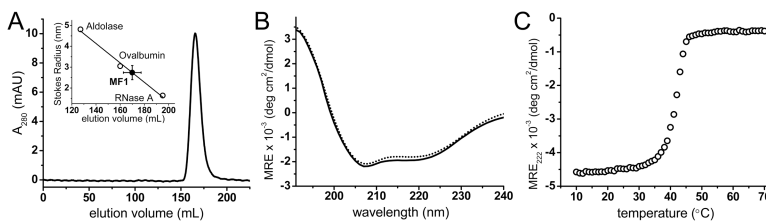


FIGURE 4. Structure and stability of MF1

(A) Gel Filtration elution profile of MF1. The elution was monitored by measuring the absorbance at 280 nm as a function of elution volume. MF1 was run on a calibrated ToyoPearl HW-55F (Tosoh Biosciences LLC) packed column with a diameter of 2.2 cm and height of 78 cm in 25 mM HEPES (pH 7.4), 50 mM NaCl, and 0.1 mM EGTA. A total of 1 mL of 0.5 – 1 mg/mL MF1 was loaded on the column with a flow rate of 1.5 mL/minute and 4 mL fractions were collected. The Stokes radius of MF1 was determined to be 2.74 ± 0.34 nm ($n=3$). (B) MF1 Far-UV CD spectrum. CD spectra were recorded in the far- (190–250 nm) UV region using a JASCO J-815 spectrophotometer with an automated temperature controller and a temperature-jacketed spectral cell. A path length of 1 mm was used with spectra recorded at 1 nm intervals for 10 μ M MF1 in phosphate buffer pH 7.0 at 25°C. Baseline scans were obtained using the same acquisition parameters with buffer alone; which were subtracted from the respective CD data scans of MF1. The raw CD signal θ_{λ} (millidegrees of ellipticity) was converted to mean residue molar ellipticity, with spectra analyzed using CDPro Analysis Software³⁰. Experimental CD spectrum (solid line) and best fit spectrum from CDPro Analysis (dotted line). (C) Thermal denaturation curve of MF1 measured by changes in mean residue ellipticity. The temperature was increased from 10 to 70°C with a step size of 1°C with the CD in millidegrees of ellipticity measured at each temperature after incubation for 2 min.